09

Optimizing the production of single-mode optical microfibers for coherent microoptics

© N.M. Lebedev,[1] K.N. Min'kov,[1] A.E. Shitikov,[1] A.N. Danilin,[1] M.I. Krasivskaya,[2] E.A. Lonshakov,[1] I.K. Gorelov,[1] N.Yu. Dmitriev,[1] I.A. Bilenko[1]

[1] Russian Quantum Center, Moscow, Russia
[2] National Research Institute, Moscow, Russia
e-mail: swanikola@gmail.com

Received February 10, 2022
Revised March 18, 2022
Accepted March 22, 2022

Micro- and nanofibers are the universal elements of the optical schemes for solving wide variety of experimental tasks. One usually uses the commercial optical fiber tapering in the burner?s flame to produce such nanofibers. Such tapers are actively used for production of highly sensitive sensors, experiments with the cold atoms and coupling to optical microresonators. The theoretical model of geometrical shape altering during the fiber tapering and heating was adapted in this publication for use in the algorithm with universal adjustment of the tapering modes to get a fiber with the desired set of parameters. One of the innovations was the implementation of the computer vision to control the tapering process. As a result, the nanofibers with the optimal waist diameter of about 700 nm for the radiation wavelength of 1.55 micron were obtained. The optimized methodic of tapering allows the production of the nanofibers with the transmittance of up to 80%. The produced nanofibers were successfully used for coupling to the crystalline whispering gallery mode microresonator. As a result, the optical combs with the spectrum range up to 200 nm were obtained in IR range..

Keywords: Nanofiber, whispering gallery mode microresonator, optical comb, fiber tapering.

DOI: 10.21883/TP.2022.06.54419.30-22

Introduction

The single-mode tapering fibers are actively [1] applied to implement interaction of light waves propagating therein with external objects in the single-mode regime. The most easy way of producing this fiber is to taper a common single-mode fiber with simultaneously heating a tapering area to the quartz softening point. As a result, a tapering fiber is produced, whose narrowest region (waist) has the interaction of the inter-fiber radiation with external optical elements at the distance less than the radiation wavelength, as in the waist the electromagnetic field substantially exits the limits of the optical waveguide. In order to implement the maximum effective interaction, it is required to obtain the optimal characteristics: a) the maximum optical transmittance in comparison with a non-tapering fiber, b) the maximum radiation intensity at the fiber-air interface (the characteristics are optimal in terms of the maximum amount of energy being transferred into the external optical element in the fundamental mode of the fiber, which is important, for example, to transmit quantum states [2]). The first condition means producing the fibers with a strictly given shape, which satisfies a adiabaticity criterion [3], of the minimum roughness and high surface cleanliness. For example, there are single examples of producing the tapering fibers with the transmittance up to 99% of the transmittance of the single-mode fiber, from which it is produced [2]. The second condition is to produce the fibers of the optimal waist diameter below 1 μm so as to obtain radiation of the wavelength of 1550 nm [4,5]. It should be also noted that in order optimize coupling of the tapering fiber with the external optical elements, it is necessary to correctly match a mode shape and a mode volume of the external element and the fiber.

For the high-Q optical microresonators with the whispering gallery modes (WGM) [6] the tapering fibers have proven themselves to be an effective coupling element, as they allow exciting the resonator modes with the minimum losses. These resonators are unique tools of the modern photonics [7]: they are actively used to create optical combs, laser sources with a narrow linewidth, electrooptic modulators, lidars [8–10]. Recently, there has been increase in interest in applying the microresonators for quantum communication and transmitting the quantum states [11]. The tapering fibers are required for successful implementation of these experiments, as the high efficiency of the fiber-resonator coupling (more than 90%) reduces the impact of parasitic noise on the system under investigation, thereby enabling, for example, measurement of the number of photons in a quantum coupling channel without absorption thereof [2]. The ultimate goal of our study is to produce the fibers suitable for the quantum measurements, which have the optimal waist diameter and the high optical transmittance (which is possible by using the procedure of optimization of the tapering fibers as described in the present study). A good indicator of applicability of the produced tapering fibers was an experiment with excitement of the optical combs therein. The optical frequency

combs are a set of equidistant lines in the spectrum representation, which are obtained based on the cascade four-wave interaction caused by the Kerr non-linearity as a characteristic of the dielectric material used to manufacture the microresonator [6]. Due to a small volume of the microresonator mode with WGM and high achievable Q factor, the generation threshold of this comb can be quite small, below 1 mW [12,13].Our observed combs with the width up to 200 nm show a high potential to use the tapering fibers in the non-linear and quantum optics.

There are various procedures for producing the tapering fibers of a different shape and diameter out of the common single-mode fiber [14,15]. Our approach uses approximation of conservation of masses and fluidity of a substance during tapering. We pre-calculate all the main parameters of the fiber and use them to make an algorithm to control the tapering on the unit. The calculations allow pre-calculating the shape of the tapering fiber, which is checked after the production using a microscope. By controlling the shape, we optimize the optical transmittance of the fiber. The computer vision algorithm proposed in the present study allows controlling the fiber tapering process by controlling the temperature within the working area by analyzing a fiber image and tuning the flame position relative to the fiber axis. Thus, despite temperature oscillations in the heated area and the different rate of the fiber diameter change at various stages of the production process, using the supposed algorithm allows stably obtaining high transmittance factors of the tapering fiber and a submicron diameter of the waist.

1. Theoretical description

Let us consider the manufacturing process for the tapering fiber in terms of getting its optimum characteristics (see Introduction). First of all, it is to get the maximum transmittance. For this, it is necessary to calculate the optimum fiber shape (in a longitudinal section) as the set of the parameters, which will be used in the tapering algorithm. Secondly, it is to find the optimum waist diameter to ensure the maximum intensity at the fiber-air interface.

Figure 1, *a* shows the typical shape of the tapering fiber and some designations used below. The waist of the fiber of the length l_w transforms to the non-tapering fiber in the transient zone of the length z_0, wherein the fiber radius is gradually changing. The waist radius is by more than two orders less than the radius of the non-tapering fiber (Fig. 1, *a*). We will strive to get the tapering fiber within the waist area to be a single-mode one for the wavelength $\lambda = 1550$ nm, which is necessary to control excitement of the certain modes in the microresonators. In order to control the number of the modes in the fiber, depending on its radius it is necessary to solve the wave equation to radiate inside its shell and core [16]. The solution is reduced to the parametrized expression for the radial components of the radiation wave inside the fiber [17]:

$$\left(\frac{J'_\nu(U)}{UJ_\nu(U)} + \frac{K'_\nu(W)}{WK_\nu(W)}\right)\left(\frac{J'_\nu(U)}{UJ_\nu(U)} + \frac{{n_{cl}}^2}{{n_{co}}^2}\frac{K'_\nu(W)}{WK_\nu(W)}\right) = \left(\frac{\nu\beta}{kn_{co}}\right)^2\left(\frac{V}{UW}\right)^4, \tag{1}$$

where U, V, W — the following parameters:

$$V = \frac{2\pi a}{\lambda}\sqrt{n_{co}^2 - n_{cl}^2},$$

$$U = a\sqrt{k^2 n_{co}^2 - \beta^2},$$

$$W = a\sqrt{\beta^2 - k^2 n_{cl}^2},$$

where $k = \frac{2\pi}{\lambda}$ — the wave number, $\beta = kn_{\text{eff}}$ — the propagation constant; K_ν, J_ν — the Bessel functions of the order ν, a — the radius of the medium, in which the radiation propagates, V — the normalized radiation frequency. The present study uses the single-mode fiber SMF-28e with the initial diameter of the core $8.2\,\mu$m and the shell $125\,\mu$m. The refraction indices of the core n_{co} and the shell n_{cl} differ insignificantly, wherein $n_{co} > n_{cl}$ (for SMF-28e $n_{co} = 1.4735$, $n_{cl} = 1.4682$ in accordance with the documentation).

The radiation propagates in the fiber in separate modes in accordance with the effective refraction index n_{eff} depending on the fiber radius. When n_{eff} is compared with the refraction index of one of the adjacent media, then the radiation goes from one medium to another (we consider 3 media: the core, the shell and air). The solutions of the equation $n_{\text{eff}}(a)$ form various modes and are designated by two letters and two digits: the first one — is the number of the mode family ν, and the second one — is the number of the mode itself. For example, the fundamental mode is designated as HE_{11}. The single-mode fiber just can have a single solution, so the light propagates only in HE_{11}. Physically, it is due to a small diameter of the core, in which only one possible angle of total internal reflection is possible.

If one starts reducing the diameter of the single-mode fiber (like in tapering), then the effective refraction index for HE_{11} will become less than n_{co} and the radiation exits to the fiber shell. It is shown on the insert of Fig. 1, *c*, representing HE_{11} in the fiber core. It can be seen that the mode will exit into the shell at the core radius of $a \approx 1.24\,\mu$m (at the same time the shell radius is $18.75\,\mu$m). At the lesser fiber radius the radiation will propagate inside the shell experiencing the total internal reflection from air already and the availability of the core can be neglected (it means that in (1) $n_{co} = 1.4682$, $n_{cl} = n_{air} = 1$, $a \leq 18.75\,\mu$m). As the value a jumps to the shell radius value, as soon as the radiation goes into it, the fiber sharply becomes the multi-mode one, with the number of the modes in proportion to $\frac{V^2}{2}$. The set of the modes in the shell with further fiber

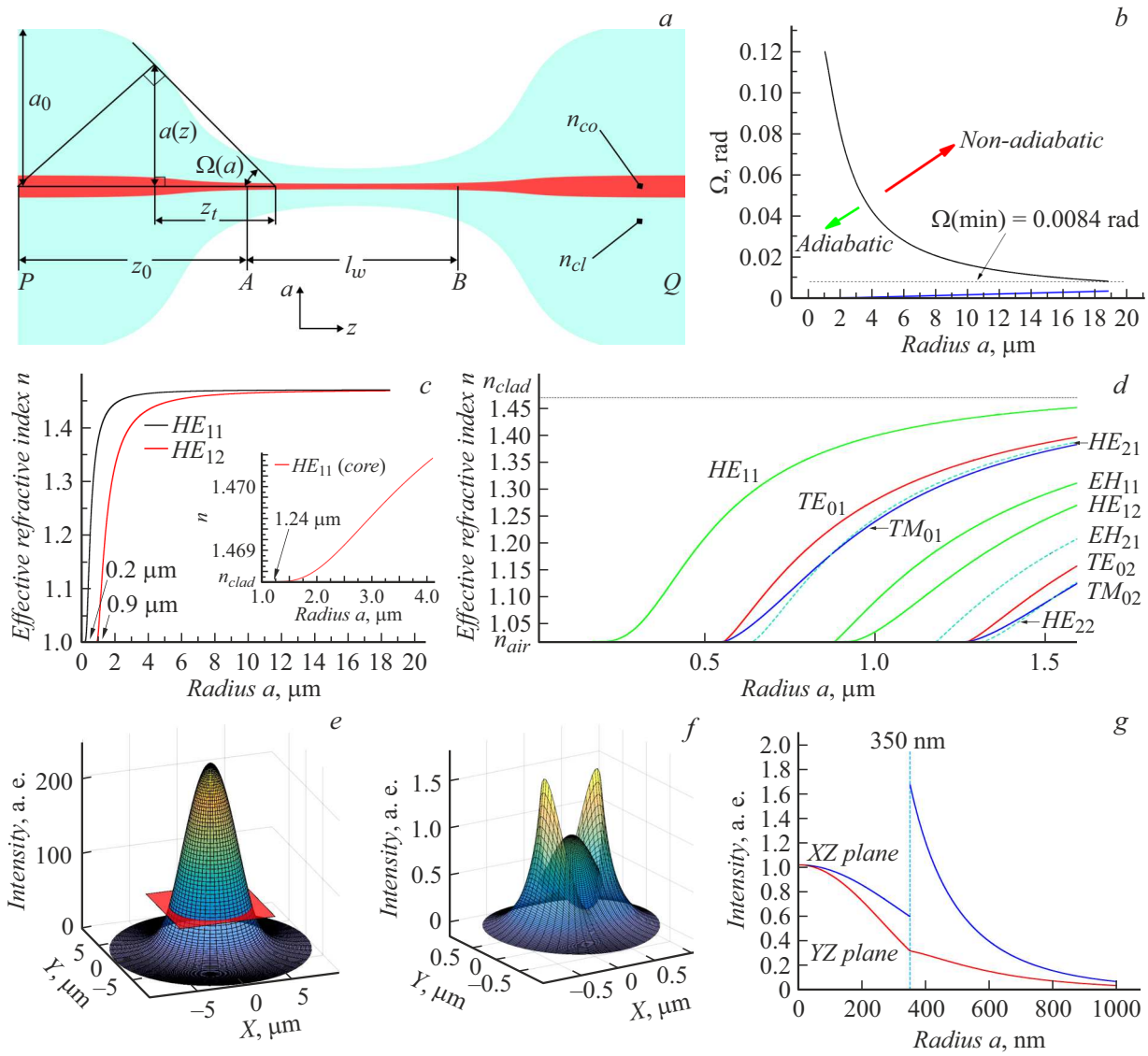

Figure 1. *a* — the typical shape of the profile of the tapering fiber, $\Omega(z)$ — the angle between the fiber axis and the tangent to its profile, $a(z)$ — the fiber profile curve; *b* — the curve of the condition of the fiber adiabaticity, the blue color shown the curve for the tapering fiber (in the online version) (see section 1.3); *c* — the adjacent modes of the same family HE_{11} and HE_{12} within the fiber shell, the insert — the fundamental mode in the core (prior to transforming to the shell); *d* — the mode family within the fiber shell at its radii from 0 to 6 μm; *e* — the intensity distribution in the section of the fiber SMF-28e; *f* — the intensity distribution within the section of the tapering fiber of the radius of 350 nm; *g* — the radiation intensity within the fiber depending on its radius and linear polarization: the blue curve — the intensity within the polarization plane, the red curve — in the perpendicular plane, the dashes designate a boundary of the fiber of the radius of 350 nm (in the online version).

tapering is shown on Fig. 1, *d*. Various families of the modes will exist there as corresponding to the different solutions of the equation (1) [17], but we are interested in the family of the fundamental modes with indices HE_{1m}, as the main energy portion is transferred exactly in them. When reducing the radius a, V is reduced until the fiber becomes the single-mode one again at the wavelength of cut-off for the fiber shell. For the SMF-28e fiber and the wavelength of 1550 nm, this regime takes place somewhere at the diameter of 1.8 μm (Fig. 1, *c*). When the fiber radius is 0.9 μm, then the last but one mode of the family of the fundamental modes HE_{12} exits into air ($n_{\text{eff}} = n_{air}$). The further tapering will result in changing the effective refraction index for the principle mode, which will gradually exit the fiber to propagate along its air boundary. Thus, in order to produce the single-mode tapering fiber, it is required to get the waist diameter of 1.8 μm for the radiation wavelength of 1550 nm.

1.1. Intensity of radiation at the fiber surface

With the diameter below 1.8 μm, the radiation intensity of the fiber surface increases [4]. With a very small diameter

of the fiber, the mode HE_{11} will fully exit into air and the intensity will be zero.

Therefore, there is an optimum waist diameter, at which the maximum intensity at the fiber surface will be attained. The intensity will also depend on the polarization of radiation in the fiber. We will consider that the radiation is linearly polarized. When calculating the dependence of the intensity on the fiber surface on its diameter, then the biggest intensity is attained approximately at the ratio $a/\lambda = 0.23$ [4,5]. Hence, we can conclude that the optimum diameter of the tapering fiber for the radiation wavelength of 1550 nm is about 700 nm. Figure 1, *e* shows the three-dimensional curve for the radiation intensity of the wavelength of 1550 nm within the cross section of the common (non-tapering) fiber SMF-28e (in the center). Figure 1, *f* — the same curve, but for the tapering fiber of the 700 nm diameter; one can observe the significant increase in the intensity at the fiber boundary in comparison with the previous one. Figure 1, *f* qualitatively illustrates the dependence of the radiation intensity on polarization: in the plane perpendicular to the polarization plane it is smaller and the radiation smoothly goes into the fiber. The polarization plane has evident sharp jump of the intensity at the fiber boundary. It shall be taken into account when operating the tapering fiber in order to obtain the maximum intensity at the fiber boundary. The curves have been obtained by numerical calculation of the distribution of the radiation intensity of the 1550 nm wavelength within the plane of the section of the fiber SMF-28e based on the equations from [5].

1.2. Adiabaticity criterion

Thus, one of the parameters of the optimum fiber has been found: it is the waist diameter of 700 nm. In order to find other parameters, it is necessary to introduce a criterion of the optimum shape (to maximize the transmittance of the tapering fiber). The typical shape of the tapering fiber is shown on Fig. 1, *a*. The AB fiber waist is connected to the non-tapering optic fiber at both sides via the transient zone PA and BQ, wherein the fiber radius is gradually decreasing. In terms of the losses, it is the transient zone that is the most problematic: it has the transition HE_{11} from the core into the shell and sharp increase in the number of the modes. At the same time, there is bond of the principle mode with higher-order modes, which are excited within the shell. The two bonded modes periodically exchange with energy at a scale of a length of beating thereof. With decrease in the shell radius, these additional modes gradually exit it. The final transmittance will depend exactly on smoothness of the transient zone profile: in order to avoid the losses, the typical beat length between the two adjacent modes z_b should be less than the typical size z_t of the tapering fiber with the radius $a(z)$ and the angle Ω of Fig. 1, *a*, otherwise the radiation will exit the fiber through the higher-order modes [3,18]:

$$z_b = \frac{2\pi}{\beta_1 - \beta_2} < z_t = \frac{a(z)}{\mathrm{tg}(\Omega)}, \tag{2}$$

where $a(z)$ — the fiber radius in each point z; β_1, β_2 — the effective constants of propagation for the adjacent modes of the same family in the fiber; $\mathrm{tg}(\Omega) \approx \Omega$ — the angle between the central axis and the tangent to the transversal fiber profile for the small values of Ω. We are interested in the losses in the fundamental mode, then β_1 — it is the propagation constant for HE_{11}, and β_2 — for the adjacent mode of its family HE_{12}. With the insufficiently smooth fiber profile, the bulk energy of the fundamental mode goes into HE_{12} (Fig. 1, *b*) [19]. By numerically calculating the adiabaticity criterion as per the results of shell mode simulation, we obtain the dependence of Ω on a. Thus, all the values of Ω below the curve will satisfy the adiabaticity criterion.

1.3. Calculation of the optimum shape

In the present study, we taper the fiber in a flame of the hydrogen-oxygen burner. As per [15], this process can be simulated by applying the laws of fluid mechanics to the glass in the heating zone. The two equations follow from [15]:

$$\frac{dr_w}{dx} = \frac{-r_w}{2L}, \tag{3}$$

$$2z_0 + L = x + L_0, \quad L_0 = L(x_0), \tag{4}$$

where L — it is the length of the heated portion, x_0 — lengthening of the fiber, r_w — the waist radius, l_w — the waist length, $a(z)$ — the fiber profile (curve), z_0 — the length of the transient zone. Thus, we have a number of parameters, which we can specify $(x_0, L(x))$ to obtain the final geometrical fiber shape $(r_w, l_w, a(z), z_0)$. And vice versa, if the required shape is known, then we can obtain the parameters for setting the unit. The simplest fiber shape $a(z)$ — it is an exponential and linear one. For these fibers we have selected the exponential shape, as it is more easy to fix a more compact fiber. The general expression for the fiber shape is specified by the integration (3):

$$r_w(x) = a_0 \exp\left(-\frac{1}{2}\int_0^x \frac{dx'}{L(x')}\right), \tag{5}$$

where $a_0 = 62.5\,\mu$m — the initial radius of the fiber. The condition $L(x) = L_0 = l_w$ will give in (6) $x = 2z$. Then, (7) will exactly specify the exponential profile:

$$a(z) = a_0 \exp\left(-\frac{z}{L_0}\right). \tag{6}$$

We specify the other parameters as $r_w = 350$ nm, $l_w = 5$ mm. From (5) for $l_w = 5$ mm we obtain $L_0 = 5$ mm, $z_0 \approx 26$ mm, $x_0 \approx 52$ mm. From Fig. 1, *b* we conclude that the condition for the angle Ω is the most rigid exactly in

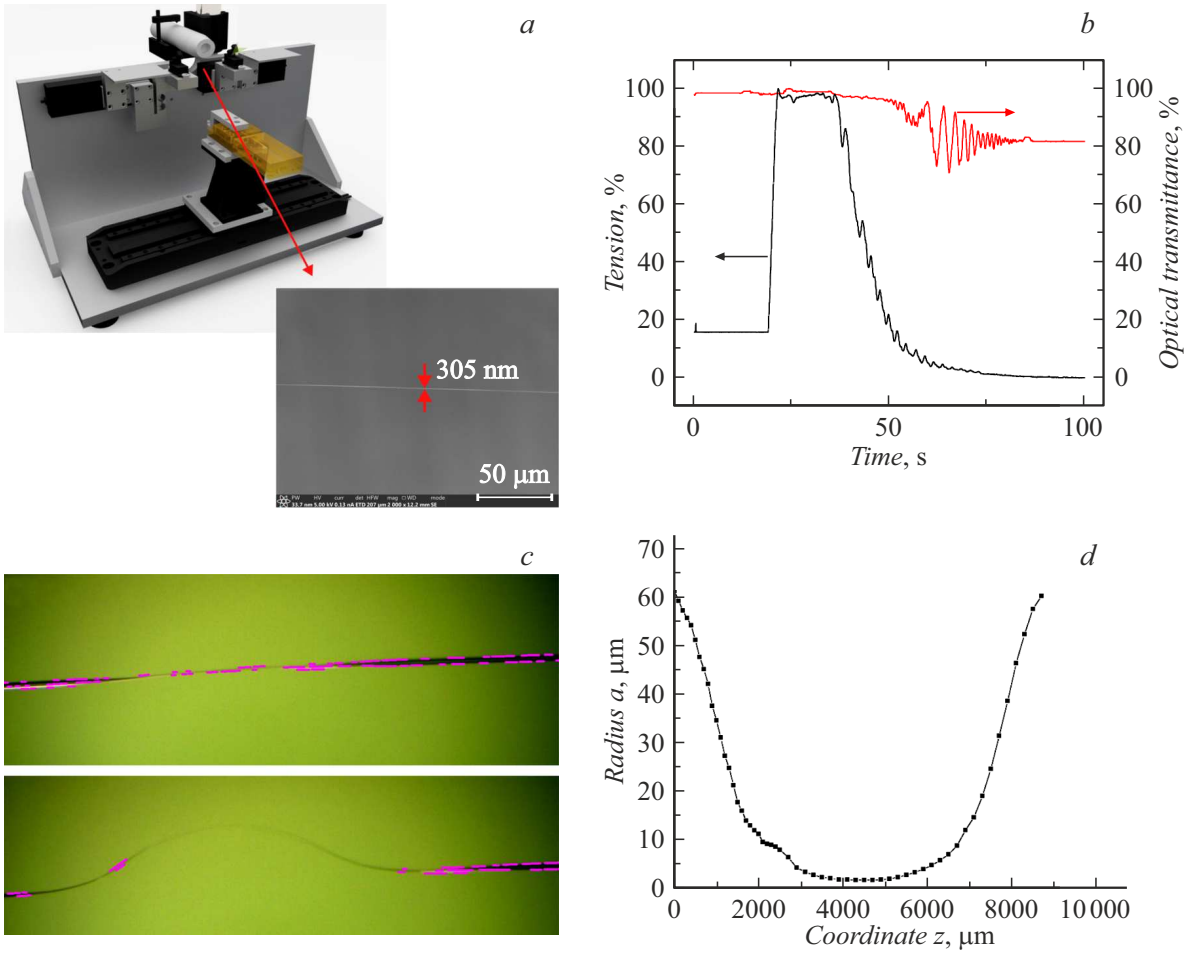

Figure 2. *a* — the general view of the unit. Below — the picture of the waist of the fiber of the 305 nm diameter in the electronic microscope; *b* — the change of optical transmittance of the fiber and its tension during tapering. The final transmittance is 80%. The 3 tapering phases mentioned in the study are well obvious; *c* — the computer vision algorithm within the OpenCV medium approximates the curvilinear profile by finding straight-line portions therein (marked with the violet color (in the online version)). Thus, the number of the straight lines and the length thereof are used as a feedback coefficient for varying an engine speed or a burner position; *d* — the map of the fiber profile with the waist diameter of the 3.6 μm, which is obtained by the optical microscope.

the point of transition of the mode HE_{11} from the core into the shell, i.e. for the adiabatic profile $\Omega \leq 0.0084$.

The total length of the tapering portion is 57 mm. The derivative $\frac{da(z)}{dz}$ will give us a tangent angle in each point. $|\frac{da}{dz}| = \frac{a}{L_0}$, the dependence $\Omega(a)$ and $|\frac{da}{dz}|(a)$ are given on Fig. 1, *b*. It is quite noticeable that the obtained parameters of the fiber shape satisfy the adiabaticity criterion, as at all the tapering stages the angle Ω is quite small (the blue curve is below the black one (in the online version)).

2. Experimental unit

When operating the fiber, we use a procedure of the moving burner [15], thereby specifying the various shape of the fiber profile. In comparison with, for example, using electrical heaters [20], the advantage of the procedure is that the components are simple and cheap as well as compact. The fiber tapering unit is designed as a structure installed on a duralumin frame with the T-shaped section (the horizonal base and the vertical plate in the middle thereof). In order to minimize the vibrations, the frame is installed on rubberized legs to a table with a ceramic granite table board. The Newport MFA-CC linear feeds are fixed in the upper part of the vertical duralumin plate and designed to taper the fiber. Both the feeds include the T-711/M-250 Thorlabs fiber clamps, which are installed coaxially. They also have platforms for additional fixing the fiber by anti-slip magnets. One of the feeds has the CAS BCL-01 strain sensor fixed to indicate fiber tension on the Keysight InfiniiVision DSO-X 2002A oscillograph. The second channel of the oscillograph is fed by a signal from the Thorlabs DET10N/M radiation detector of the ECDL10620R laser to control the fiber transmittance factor. The fiber is heated by the gas burner fixed on the Thorlabs DDS-220/M feed, which is designed to move the burner

flame along the fiber. The oxygen and hydrogen mixture is provided by the LIGA-02S electrolyzer, which is capable of adjusting the gas flowrate by a rotameter. The three-dimensional model of the unit is shown on Fig. 2, *a*.

The tapering parameters, i.e. the length of the heating area L_0, the coefficient of the length heating change α, the minimum heating length L_{fin}, the burner swinging rate V_{brush} have been specified in the process control software. The distance between the flame and the fiber, as well as the fiber tapering rate v have been adjusted manually directly in the tapering. The tapering process is controlled by the microscope with a digital camera. It is exemplified on Fig. 2, *d* by showing the map of the tapering fiber profile with the waist diameter of $3.6\,\mu$m. Due to using the optical microscope for measurement of the profile shape, the possible measurement error can be up to $1\,\mu$m. The main tapering parameters are selected to get the adiabatic profile of the exponential shape: $v = 0.04$ mm/s, $L_0 = 1$ mm, $V_{brush} = 1$ mm/s.

3. Tapering procedure

The tapering process starts with preparation of the fiber portion: the polymer shell is peeled off it and its remnants are removed by means of a lint-free tissue soaked in acetone. Then, the fiber is fixed in the clamps and additionally pressed to the platforms by means of the magnets in order to prevent slippage through the clamps. One of the necessary conditions of the qualitative result is co-axiality of the clamps and movement of the burner in parallel to the fiber axis at each moment of time. Then the electrolyzer is switched on to adjust the flowrate of the gas mixture ($0.2-0.3$ l/min) and the distance between the burner and the fiber ($1-25$ mm). The above-listed parameters are set. Before the start of tapering, the feeds are pushed apart by 0.2 mm each, in order to ensure uniform fiber tapering at the beginning of the process. Then, the burner swinging, its flame ignition and pushing apart the fiber fixtures are simultaneously switched on. In tapering, the important parameter is fiber tension, from which the transmittance depends at the initial stages. In order to control the fiber tension in the manual mode, one can shift the flame along the height and change the rate v.

The whole tapering process can be divided into the 3 phases (Fig. 2, *b*): the phase 1 (small transmittance drop), the phase 2 (transmittance oscillations), the phase 3 (getting to the constant transmittance). It was noted that pre-heating the fiber in the burner flame during 5 s prior to starting the tapering process helps reduce the transmittance losses. In the first stage, the burner flame is set to be by $1-2$ mm closer so as to better heat up the fiber. In transition into the second stage, the tension sharply drops. By smoothly reducing the tension by increasing the distance from the flame to the fiber, it is possible to obtain the lesser drop of the transmittance. Then, in transition to the third stage, the fiber starts sharply reducing in the diameter and buckling upwards. That is why one can increase the tapering rate at this moment [21] in order to keep the fiber straight. It prevents premature breaking of the fiber and its shape asymmetry. When the last non-fundamental mode exits the fiber, one can notice typical reduction of the amplitude of the transmittance oscillations. Using this point, it is possible to determine the fiber diameter ($1.8\,\mu$m for the wavelength of 1550 nm) [20]. In further tapering, the fiber diameter becomes less than $1\,\mu$m and the fundamental mode starts smoothly exiting the fiber. By determining the right moment and stopping the tapering process, it is possible to obtain the fiber of the diameter of up to several hundreds nm without the transmittance drop with the maximum intensity of radiation at the boundary. Otherwise, the transmittance starts sharply dropping and the fiber breaks. With successful tapering, the residual sagging of the fiber slowly pulls up by small step. An important feature for increasing the transmittance by 20% and more has turned out to be fiber cleaning by a methanol drop from the Schuster trickle after tapering: the fiber is submerged into the drop at the trickle tip, which cleans the tapering portion when cautiously moving along the fiber axis. It helps get rid of microparticles, which can hit the fiber surface in tapering. Then, the fiber is glued into a duralumin holder by means of an UV-glue. The UV radiation is performed for 20 min at the power of 10 mW in order to avoid collapse (then the power is increased to 360 mW for full solidification). Then the microscope test the fiber waist diameter, its shape and the waist length.

4. Optimization of transmittance factor

The main reasons for the losses of tapering transmittance are a very sharp drop of tension in transition into the phase 2. In turn, it results in the increased amplitude of the transmittance oscillations, thereby reducing its final value. In order to prevent this drop, it is necessary to correctly select the flame temperature and fiber tension in the phase 1. In order to control the tension, it is suggested to use the strain sensor built into the unit. It is also not easy to set the flame temperature as the gas mixture from the electrolyzer has impurities of electrolyte vapors and a non-constant gas ratio for the gases H_2 and O_2. To overcome this, we have provided the gas mixture supply system with a drier and a liquid gate to be filled with methanol. It allowed obtaining a more stable and hot flame. It has been also found that a heating source should have been sufficiently localized so as to avoid contact of flame with the fiber (otherwise, it would instantaneously melt). However, the heating area temperature should be sufficiently high for its softening ($> 1500^\circ$C). That is why we have used a nozzle made of a medical needle with the internal diameter of 0.3 mm and the minimum possible current at the electrolyzer plates, at which it is possible to ignite the mixture. Here, a certain danger is mixture detonation inside hoses of the supply system at a very

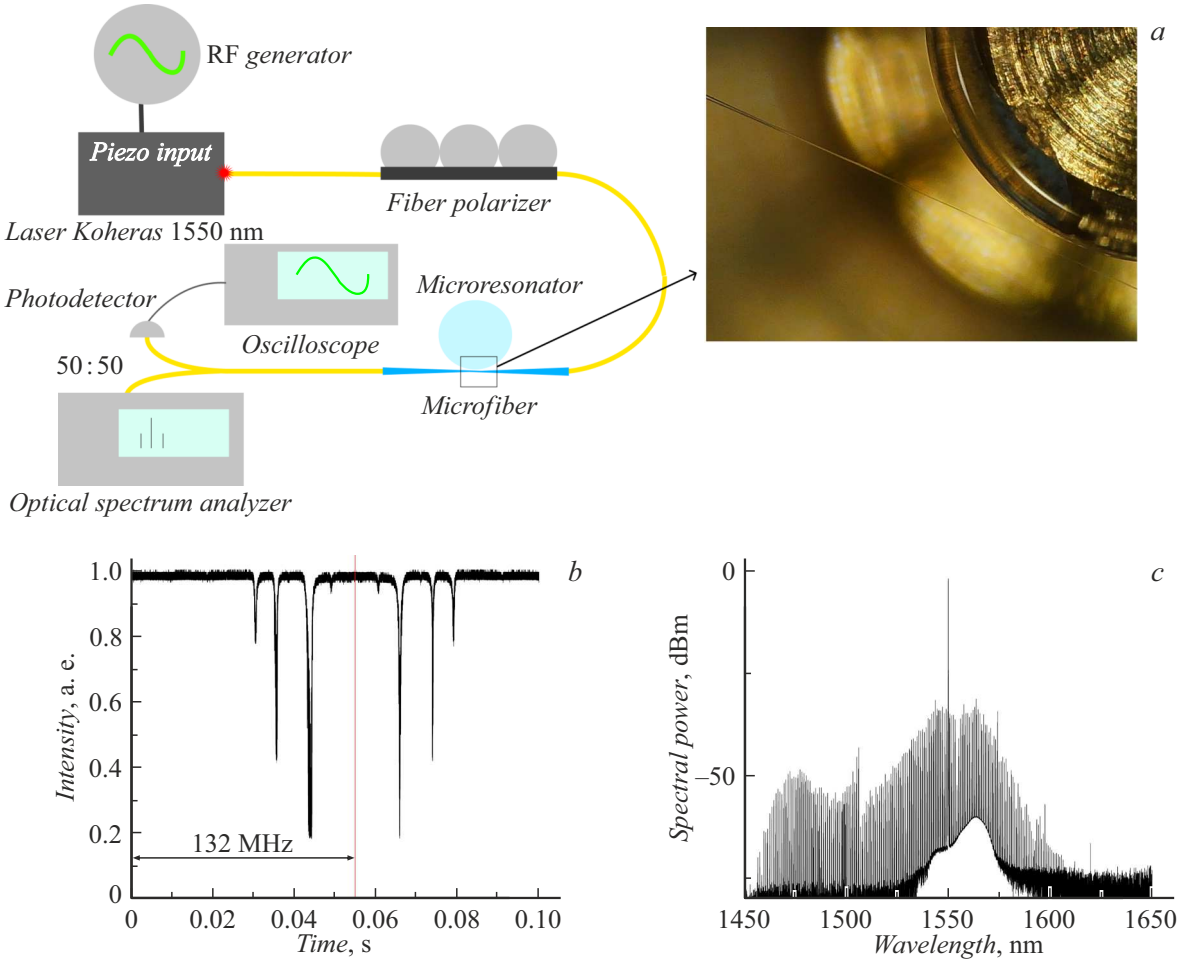

Figure 3. *a* — the view of the unit for checking the coupling of the microresonators with the tapering fibers. To the right — the picture of the microresonator with the brought fiber; *b* — the mode spectrum of the microresonator when scanning as per the frequency directly and reversely at 132 MHz around the wavelength of 1550 nm; *c* — the examples of the optical combs produced by pumping to 80 mW at the optical spectrum analyzer. The combs were produced by additionally using the Koheras Boostik amplifier.

weak flame. That is why it is mandatory to use the liquid gate. An important feature for increasing the final transmittance was selection of the correct burner swinging rate V_{brush}. At the very high rates the fiber fails to heat up, while at the small ones — the profile loses its symmetry. A significant feature includes no fiber sagging during the tapering phase 3. Finally, the critical moment is to stop the process and further additional tension of the fiber to avoid the sagging.

In order to take into account all these features, an original software version has been developed to manually adjust the fiber tension and the tapering rate by turning a supply handle in dependence on oscillograph readings. However, this approach is less efficient in repeatability, so the software has been modified. The second version includes automatic changing of the tapering rate as per pre-set values depending on an engine coordinate. It allows setting the unit for the continuous operation mode, but requires larger time intervals, as all the parameters are selected empirically. That is why it was proposed to use the computer vision algorithm designed to determine the fiber bending by the camera image and change the tapering rate in the phase 3 or the burner position so as to control the tension in the phase 1. The respective algorithm has been implemented in two options: by the NI Vision Development Module and in the Python language by means of the OpenCV library.

The first option has used a built-in function of curve profile reading, thereby arranging the feedback directly in LabView. However, this option is of quite complicated architecture and has a large scope of resources used. The second option?s algorithm has calculated the number and the length of the straight lines (Fig. 2, *c*), which approximated the fiber?s curvilinear profile in the real-time mode on a video camera?s video frame. The image was processed by using the canny filter functions. The advantage of this approach is usability of the commercial microscopes with the Levenhuk type camera, as it is not mandatory to clearly resolve the image at each moment within the area of fine fiber waist, and the fiber profile curvature can be also traced by means of the bending in the transient zone.

It allows tracing the excessive curvature of the fiber in the tapering phase 3. When the profile curvature is increased, the number and the length of the lines are reduced. By building the parameter corresponding to the curvature into the feedback system, it is possible to increase the engine speed or shift the burner flame relative to the fiber axis in order to maintain the uniform tapering process. Both the options have been successfully tested on the video files of the fiber tapering process.

5. Results

By applying the above-described procedures, we have succeeded to produce the fibers with the transmittance factor up to 80%. Furthermore,the accurate control of the tapering time has enabled producing the waists of the diameter of up to several hundred nanometers. It has been confirmed by the images on the electron microscope and a process chronology recorded by the oscillograph (Fig. 2, *a,b*).

The computer vision has been successfully integrated into the tapering algorithm and checked by the video files of the tapering process. The Labview medium allows using this modification in order to control any unit parameter affecting the fiber tapering process.

The fiber quality has been checked by using the unit for implementing the optical coupling with the crystal microresonator.

The tapering fibers were successfully used to couple to the WGM microresonator of the 3.63 mm diameter. Using the unit of Fig. 3, *a*, the tapering fiber?s waist was brought to the microresonator boundary and the whispering gallery modes were excited in it, which were observed by frequency tuning of the laser within the 132 MHz range around the wavelength of 1550 nm. The obtained spectrum when increasing and decreasing the laser frequency is shown on Fig. 3, *b*. The mode contrast of the critical coupling exceeded 80%. At the pumping power of 80 mW, we observed the optical frequency comb. In order to excite the frequency comb, we switched off the pumping laser frequency retuning and provided for the required detuning. The comb spectrum is shown on Fig. 3, *c*. Probably, the spectrum asymmetry was caused by the fact that the optical fiber has the transmittance boundary of 1620 nm. The comb width can be up to 200 nm. Thus, the tapering fibers with the WGM microresonators can be successfully applied for various applications correlated to the spectroscopy, the lidars and the quantum measurements [2,8].

Conclusion

A number of novelties has been successfully implemented and tested to simplify the tapering process, facilitate its repeatability and allow manufacturing the high-quality tapering fibers. The fiber efficiency was demonstrated in WGM excitement in the high-Q optical microresonators. The high efficiency of the fiber-resonator coupling enabled demonstrating the optical combs with the width up to 200 nm. These fibers can be successfully used for application in the fields of the quantum and non-linear optics. The technical novelties implemented in the study include a diagram of automatic removal of the burner in case of the tapering stop. It also included solving the problem of insufficient fiber tension after the process stop. It has been shown that flushing the tapering fiber in methanol can increase the transmittance factor by more than 20%. The computer vision method has been successfully implemented to control the bending of the tapering fiber in real time.

In the future, as a result of optimization of all the three phases of the tapering process, including deeper integration of computer-aided learning, it is planned to manufacture the tapering fibers with given characteristics with the transmittance above 99% to be suitable for observing the quantum effects.

Funding

This study was carried out under partial financial support of the RSF (the grant № 20-12-00344).

Conflict of interest

The authors declare that they have no conflict of interest.

References

[1] L. Tong, F. Zi, X. Guo, Lou. J. Opt. Commun., **285**, 4641–4647 (2012).
[2] P. Solano, J.A. Grover, J.E. Hoffman, S. Raverts, F.K. Fatemi, L.A. Orozco, S.L. Rolston. Adv. At. Mol. Opt. Phys., **66**, 439–505 (2017). https://doi.org/10.1016/bs.aamop.2017.02.003
[3] S. Lacroix, R. Bourbonnais, F. Gonthier, J. Bures. Appl. Opt., **25**, 4421 (1986).
[4] F. Warken, E. Vetsch, D. Meschede, M. Sokolowski, A. Rauschenbeutel. Opt. Express, **15**, 11952 (2007).
[5] F. Le Kien, J.Q. Liang, K. Hakuta, V.I. Balykin. Opt. Commun., **242**, 445–455 (2004).
[6] M.L. Gorodetsky. *Opticheskie microrezonatory s gigantskoj dobrotnost?yu* (Fizmatlit, 2011), 416 p. (in Russian).
[7] T.A. Birks, W.J. Wadsworth, P.St.J. Russell. Opt. Lett., **25**, 1415–1417 (2000).
[8] S.M. Spillane, T.J. Kippenberg, O.J. Painter, K.J. Vahala. Phys. Rev. Lett., **91**, 2–5 (2003).
[9] G. Brambilla, F. Xu, P. Horak, Y. Jung, F. Koizumi, N.P. Sessions, E. Koukharenko, X. Feng, G.S. Murugan, J.S. Wilkinson, D.J. Richardson. Adv. Opt. Photon., **1** (1), 107–161 (2009).
[10] G. Sague. *Cold Atom Physics Using Ultra-Thin Optical Fibre* (Rheinischen Friedrich–Wilhelms–Universit, Bonn, 2007), 164 p.
[11] S.M. Spillane. Fiber-coupled Ultra-high-Q Microresonators for Nonlinear and Quantum Optics Thesis by. Thesis 2004, 143 (2004).

[12] A. Pasquazi, M. Peccianti, L. Razzari, D.J. Moss, S. Coen, M. Erkintalo, R. Morandotti. Phys. Reports, **729**, 1–81 (2018).
[13] M. Kues, C. Reimer, J.M. Lukens, W.J. Munro, A.M. Weiner, D.J. Moss, R. Morandotti. Nature Photonics, **13** (3), 170–179 (2019).
[14] F. Warken. Ultradünne Glasfasern als Werkzeug zur Kopplung von Licht und Materie. Thesis 1–183 (2007).
[15] T.A. Birks, Y.W. Li. J. Light. Technol., **10**, 432–438 (1992).
[16] E. Vetsch. Optical Interface Based on a Nanofiber. 152 (2010).
[17] A.W. Snyder, J. Love. *Optical Waveguide Theory* (Academic Publishers, Kluver, 1983)
[18] J.D. Love. IEE Proceedings. Part J., Optoelectron., **136** (4), 225–228 (1989). DOI: 10.1049/ip-j.1989.0037
[19] J.D. Love. Electron. Lett., **23**, 993–994 (1987). DOI: 10.1049/ip-j.1989.0037
[20] Y. Yu, X. Zhang, Z. Song, J. Wang, Z. Meng. Appl. Opt., **53** (35), 8222 (2014). https://doi.org/10.1364/AO.53.008222
[21] J.E. Hoffman, S. Ravets, J.A. Grover, P. Solano, P.R. Kordell, J.D. Wong-Campos, L.A. Orozco, S.L. Rolston. AIP Adv. **4**, 067124 (2014). https://doi.org/10.1063/1.4879799